Metastable refractive index manipulation in hydrogenated amorphous silicon for reconfigurable photonics

Document status and date:
Published: 01/03/2020

Document Version:
Publisher's PDF, also known as Version of Record (includes final page, issue and volume numbers)

Please check the document version of this publication:

• A submitted manuscript is the version of the article upon submission and before peer-review. There can be important differences between the submitted version and the official published version of record. People interested in the research are advised to contact the author for the final version of the publication, or visit the DOI to the publisher's website.
• The final author version and the galley proof are versions of the publication after peer review.
• The final published version features the final layout of the paper including the volume, issue and page numbers.
Link to publication

FULL PAPER

ADVANCED
OPTICAL
MATERIALS
www.advopticalmat.d

Check for
updates

Metastable Refractive Index Manipulation in Hydrogenated Amorphous Silicon for Reconfigurable Photonics

*Mahir Asif Mohammed, Jimmy Melskens, Ripalta Stabile, Francesco Pagliano, Chenhui Li, Wilhelmus M. M. Kessels, and Oded Raz**

Hydrogenated amorphous silicon (a-Si:H) is known for exhibiting light-induced metastable properties that are reversible upon annealing. While these are commonly associated with the well-known deleterious Staebler–Wronski effect in the field of thin-film silicon solar cells, the associated changes in optical properties have not been well studied. Emerging reconfigurable photonic devices and applications can benefit from metastable optical properties where two states of the material are reversibly accessible without the need for continuous stimulation. The study demonstrates a light-induced 0.3% increase of the metastable refractive index of a-Si:H that is reversed upon annealing over several cycles using a highly sensitive Fabry–Pérot interferometric technique. Utilizing this technique, a metastable optical switch based on a micro-ring resonator is demonstrated with reversible distinct switching states separated by 0.3 nm between the light-soaked and annealed states, a switching extinction exceeding 20 dB and an unchanged Q-factor, suggesting no excess discernible optical loss. Furthermore, metastable strain changes in a-Si:H-based freestanding membrane structures are linked to the observed metastable optical properties and present a possible route to stable photonic devices. Our proof-of-concept demonstration showcases a-Si:H-based reconfigurable photonics that support multiple purpose photonic integrated circuits, reconfigurable metamaterials, and advanced optomechanical devices.

1. Introduction

Reconfigurable or programmable generic photonic integrated circuits (PICs) have been identified as a key enabling technology toward smart photonic systems that can be accessed by users or designers to perform a multitude of functionalities.[1,2] Such programmable multifunctional PICs have been suggested as building blocks in applications such as signal processing, quantum logic gates, deep learning, lab-on-chip, optical memory, smart display, etc.[3–10] Responsive optical materials that allow programming of their refractive index between two or more stable states are key to achieving reconfigurable photonic devices. Conventional techniques involve the exploitation of the volatile thermo-optic or free-carrier dispersion effects in various materials. However, these techniques might require continuous power supply (0.25 W per heater), intricate solutions for associated heat dissipation challenges, and complex control circuits.[2] Alternatively, materials that offer a non-volatile change in the refractive index post-stimulation have been integrated with photonic devices.[11–14] Among these, optical-phase changing materials (O-PCMs) have received significant attention in the field of reconfigurable photonics lately, as these offer on-chip programming with a reversible change in refractive index (Δn).[9,10,14–18] These materials have their own limitations owing to increased optical losses due to high absorption with respect to the O-PCM (e.g., $Ge_2Sb_2Te_5$ [GST]) switching state.[9,19] Recently, some efforts have been made for realizing low-loss programmable photonic devices with new device architectures and material combinations.[16,20] Yet, there remains a need to find a material with metastable optical properties that can be switched between states without suffering from excess loss and that has a self-holding property of the programmed states.

Early work on hydrogenated amorphous silicon (a-Si:H) by Staebler and Wronski uncovered the light-induced metastability of the material, whereby a reduction of the photoconductivity is observed when exposing the material to light that can be partially reversed by a subsequent long-term annealing treatment in the dark.[21,22] Follow-up investigations have also indicated reversible Si-Si binding energy changes, Si–H

M. A. Mohammed, Dr. R. Stabile, Dr. C. Li, Dr. O. Raz
Electro-Optical Communication Group
Department of Electrical Engineering
Eindhoven University of Technology
P.O. Box 512, 5600 MB Eindhoven, The Netherlands
E-mail: o.raz@tue.nl
Dr. J. Melskens, Prof. W. M. M. Kessels
Plasma and Materials Processing Group
Department of Applied Physics
Eindhoven University of Technology
P.O. Box 512, 5600 MB Eindhoven, The Netherlands
Dr. F. Pagliano
Photonics and Semiconductor Nanophysics
Department of Applied Physics
Eindhoven University of Technology
P.O. Box 512, 5600 MB Eindhoven, The Netherlands

The ORCID identification number(s) for the author(s) of this article can be found under https://doi.org/10.1002/adom.201901680.

vibrational absorption changes, and specific heat and internal friction changes that suggest structural changes in the material.[23–25] Experiments using a beam from a high-intensity laser on cantilevers made of a-Si:H have offered experimental support for this suggestion with a measured metastable volumetric expansion that is reversible between the light-soaked and annealed states.[26,27] Consequently, the relation between these metastable properties and the optical properties (refractive index, n and extinction coefficient, k) was characterized using spectroscopic ellipsometry (SE), predominantly in the UV spectrum.[28,29] While considerable scientific effort has been spent on investigating the phenomenon in photovoltaic cells, its potential application for reconfigurable photonics by exploiting the metastable optical properties has remained unexplored.[30–33]

Despite being considered a deleterious effect for thin-film silicon solar cells, we propose that the Staebler-Wronski effect (SWE) can be exploited to facilitate a novel pathway toward reconfigurable photonic devices. First, we discuss a specifically designed and fabricated thin-film Fabry-Pérot (FP) interferometric system. The FP device was used to study the effects of annealing and high-intensity light soaking cycles on the optical properties of a-Si:H in the near-infrared part of the spectrum (around 1550 nm). After observing initial irreversible changes in refractive index, n, a reversible change can be realized that is sufficient to demonstrate reconfigurable photonic integrated switches and filters. We discuss the possible reasons behind the initial irreversible changes in n based on careful material analysis. We proceed to demonstrate a metastable optical switch based on a micro-ring resonator (MRR) made of a-Si:H of similar composition, that exhibits two distinct switching states corresponding to the annealed and light-soaked states over the course of multiple cycles. The change in the refractive index comes at no discernible increase in optical loss for the optical switch; however, we observed long-term instability with the programmed state of the device. To understand the source of the metastable refractive index change and better understand the instability, we studied the effects of annealing and light soaking on freestanding a-Si:H thin-film membranes. We demonstrate that the freestanding membranes exhibit metastable intrinsic strain modulation that can be related to the observed metastable refractive index change found in the FP and ring resonators experiments. In addition, long-term stability was demonstrated for the freestanding membranes opening the path for making stable photonic devices. Finally, we discuss potential aspects that should be considered for further development of the technology in order to realize reconfigurable PICs with metastable a-Si:H.

2. Results and Discussion

2.1. Thin-Film Interferometry

An interferometric technique based on thin-film FP cavities was adopted to study the minute changes resulting from annealing and high-intensity prolonged light soaking on a-Si:H. Strong constructive or destructive interferences can be realized when multiple reflections from thin-film interfaces are

phase-matched appropriately.[34,35] Frequency, angle, and polarization of light along with thicknesses and refractive indices of the thin films are all relevant parameters for designing such a resonant structure. Here, a thin-film stack consisting of a-Si:H (265 ± 0.6 nm) on SiO$_2$ (119.5 ± 0.5 nm) was fabricated as per the design to form the destructive interference that is commonly referred to as an anti-reflection (AR) coating in the near-infrared spectrum (as shown in **Figure 1**a). The error margin indicated here corresponds to statistical error determined from spectroscopic ellipsometric (SE) measurements of the fabricated AR coating. The model used for designing the AR stack is described in Section 1, Supporting Information. The choice of designing an AR coating in the near-infrared was due to the fact that the majority of PICs are fabricated and used in this wavelength range (related to the low absorption of light with a wavelength above 1100 nm in silica-based optical fibers). The schematic of the measurement setup is shown in Figure 1b. The sample holder was maintained at 20 °C throughout the measurement. The sample was placed on the holder and a vacuum pump was used to maintain the position of the sample. A tunable laser source (1465–1575 mn) was used to scan the wavelength with a resolution of 0.1 nm. Laser light guided through a polarization-maintaining fiber (PMF) was collimated by a fiber collimator. Then the 3 mm collimated beam was launched through a polarization filter on the sample and reflected light was collected by a power meter. The sample holder was held on a rotatable mount so that the optimum angle can be set for obtaining minimum reflection. At an incidence angle (θ_i) around 11.3°, the measured response as reflectance from the resonant structure is shown in Figure 1c. The reflectance reached its minimum because of the maximum destructive interference at 1508.65 nm. Simulations show a good fit with the measured reflectance considering the refractive indices ($n_{\text{a-Si:H}} = 3.184$; $n_{\text{SiO}_2} = 1.456$) and thicknesses of the thin films (a-Si:H: 265.6 nm; SiO$_2$: 119.5 nm) determined by SE measurements. These resonant devices are extremely sensitive to changes in refractive index (n) and/or thickness (d) of the a-Si:H film. Hence, similar devices are suggested for switchable high-resolution reflective color displays based on O-PCM.[10,18,36,37] A simulation of the sensitivity of the structure (Figure 1d) shows that for an increase in n as small as 0.1%, a red-shift of the reflectance minimum position by 1.55 nm is obtained, while a blue-shift is observed if n decreases by 0.1%. Similarly, a 0.1% decrease in d will result in a blue-shift by 1.3 nm and vice versa for an increase in d. Therefore, this resonant device is suitable for studying any minute changes that may be induced by annealing and light soaking.

The measurement setup was made in such a way that it was possible to perform light soaking without moving any parts of the systems. The lamp could be carefully placed and removed without disturbing any components. In addition, the sample was placed on a marked position to ensure measurement on the same spot after annealing. Measurements were performed as the sample holder temperature was maintained at 20 °C after annealing and light soaking steps. The experiment started with an as-fabricated resonant device and the reflectance minimum wavelength was recorded to be 1508.65 nm as shown in **Figure 2**a. The as-fabricated device showed a blue-shift of 0.15 nm (1508.50 nm) within 26 h of
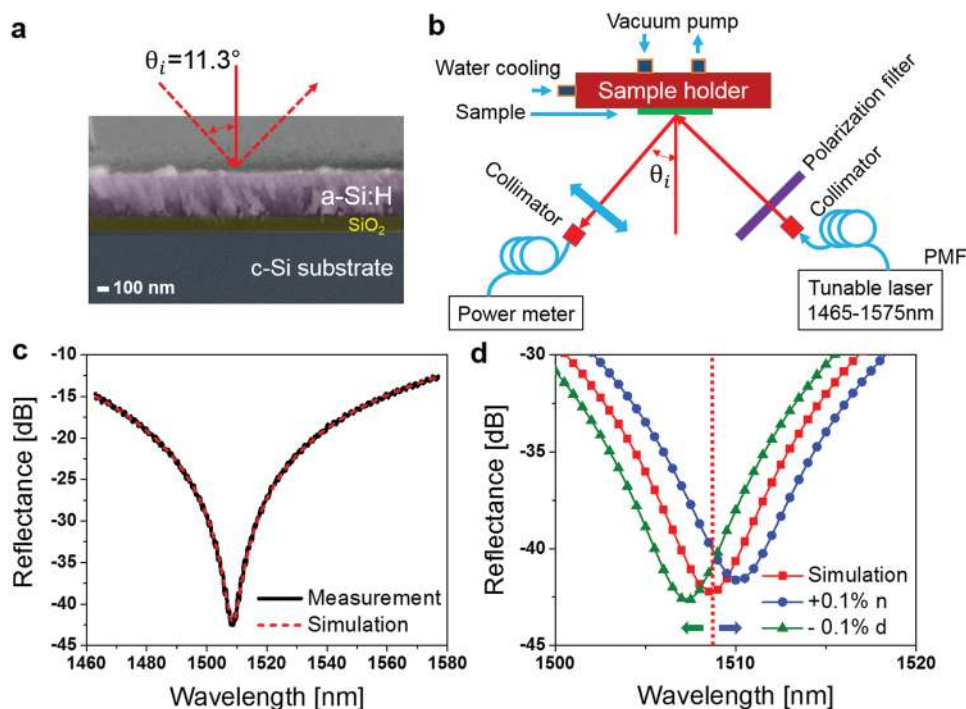
Figure 1. Thin-film interferometric device and measurement setup. a) The resonant device was fabricated with predefined a-Si:H and SiO$_2$ thicknesses on a silicon substrate as shown by the SEM cross-section image. At a certain angle of incidence ($\theta_i = 11.3°$) and wavelength, destructive interference will occur, yielding a sharp reflectance minimum. b) The schematic of the measurement setup is shown here. Collimated and polarized light from a tunable laser (1465–1575 nm) was used to scan the wavelength and measured reflected power at a power meter from the sample. PMF, polarization maintaining fiber. c) The reflectance measurement shows a steep drop in intensity at a certain wavelength that corresponds to the destructive interference condition. The simulation matches well with the measurement. d) The resonant device is extremely sensitive to minute changes in internal (refractive index, *n*) and external (film thickness, *d*) properties (simulation).

aging that was sustained even after annealing the sample for the first time. A blue-shift of 2.20 nm (1506.30 nm) was observed after annealing the sample at 180 °C for 4 h in N$_2$ environment. Aging 250 h after annealing, a slow blue-shift of 0.40 nm (1505.90 nm) was observed. The sample was light-soaked for 300 h until saturation of the blue-shift effect that was measured to be 1.05 nm (1504.85 nm). Annealing the sample yet again showed another blue shift of 0.95 nm (1503.90 nm). Until this point, we observed only blue-shifts of the reflectance minimum wavelength position from the as-fabricated position by a combined shift of 4.75 nm in total. However, the next light-soaking period resulted in a 0.40 nm red-shift (1504.30 nm), indicating the onset of reversibility of the position of reflectance minimum. From here onward, annealing resulted in a blue-shift of the reflectance minimum wavelength that can be reversed by light soaking and the magnitude of reversibility is around 0.4 nm, as is shown in Figure 2a. Interesting to note is that the light-induced reversibility clearly saturated after 120 h of light soaking. Also, the data points corresponding to the annealed states showed a saturating behavior after the sample was passed through a couple of annealing steps. This suggests that the repeatability of the reversibility improves after a couple of cycles of annealing and light soaking. Finally, there was an aging period of 35 h after the last annealing treatment that showed the stability of the measured state, unlike the initial aging periods that resulted in blue-shifts.

It is possible that the initial irreversibility is related to a higher extent of change (a larger magnitude) that conceals the comparatively smaller light-induced reversibility. Oxidation of the surface and loss of hydrogen were reported to cause a decrease in the refractive index, and therefore can be related to the observed initial irreversibility manifested as blue-shift. Interestingly, this observation is similarly made for the thin-film solar cells as there is also an initial onset of degradation of the photoconductivity and solar cell efficiency that cannot be recovered by annealing after light soaking.[38] The reversibility and repeatability improved once these irreversible changes took place. The changes in the effective refractive index after each cycle of annealing and light soaking treatments are shown in Figure 2b. As expected, the initial irreversible blue-shift corresponds to a decrease of the effective refractive index. The red-shift associated with light soaking is linked with an increase of the effective refractive index and the reversible effective refractive index change (Δn) is estimated to be around 0.001. It is important to mention that no distinguishable signs of increased optical loss due to annealing or light soaking were observed (such as decreased extinction or broadening of AR resonance).

In parallel with the measurements reported above, we also performed Fourier transform infrared spectroscopy (FTIR), X-ray photoelectron spectroscopy (XPS), and Raman spectroscopy measurements to isolate the factors contributing to initial irreversibility. FTIR spectroscopy is a popular characterization technique for a-Si:H to determine hydrogen content, mass
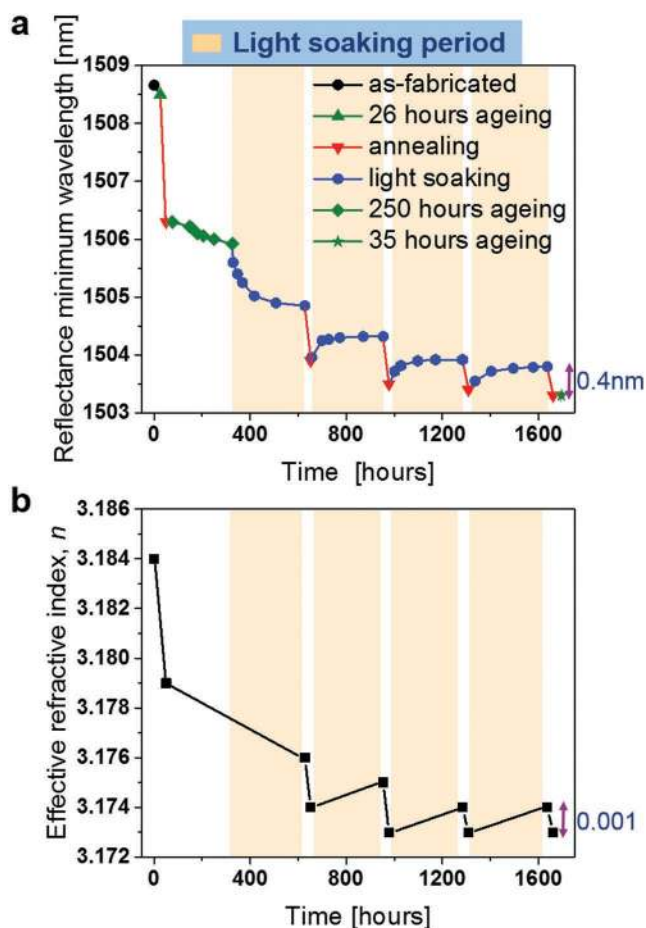
Figure 2. Annealing and light-soaking experiment with thin-film interferometry. a) The shift of the measured reflectance minimum position as the sample goes through cycles of annealing and light-soaking treatments (1 cycle = 1 annealing and 1 light-soaking treatments). After a few irreversible steps in the beginning, reversibility was observed by 0.4 nm. b) Effective refractive index change obtained from fitting of the measured data after each annealing and light-soaking treatment. The reversibility observed in reflectance minimum wavelength shift can be translated as an effective refractive index change by 0.001.

density, and microstructure parameters that are relevant to assess the presence and distribution of vacancies and voids in the film.[32,39,40] The lower stretching mode (LSM) and higher stretching mode (HSM) vibrational absorptions characteristics of silicon hydride (Si–H$_x$) bonds can be found around 2000 and 2100 cm^{-1}, respectively. LSM is associated with silicon monohydride bond (Si–H) and HSM is associated with silicon hydride bonds (Si–H$_x$) around vacancies and nano-sized voids (see Figure S3a, Supporting Information).[33,39–41] In addition, we investigated the change in silicon oxide (Si–O) stretching mode absorption change from the FTIR measurements. The characteristic band peak around 1075 cm corresponding to in-phase stretching mode absorption and a broad shoulder around 1130–1150 cm^{-1} corresponding to out-of-phase stretching mode absorption are shown in Figure S3b, Supporting Information.[42] From the FTIR measurements corresponding to cycles of annealing and light soaking on the AR-coating, it is evident that the Si–H peak absorbance decreases from

its as-deposited condition after the first annealing and continued to decrease after first light soaking as well (as shown in Figure S3c, Supporting Information). Subsequently, stability is observed after more annealing and light-soaking cycles. This is a clear indication of the loss of hydrogen during annealing and light soaking that was reported from the study of light-induced degradation of thin-film silicon solar cells.[43,44] From the measurements, the increase in Si–O peak absorbance after the first cycle of annealing and light-soaking treatments is clearly visible as is the unchanged nature of these peaks afterward (as shown in Figure S3c, Supporting Information). As a result, it can be concluded that there is an increase in Si–O species on the as-deposited film after annealing and light soaking. Bare a-Si:H is expected to go through surface oxidation, hence the observed Si–O changes may be only related to surface oxidation. Subsequently, XPS measurements were also performed that are limited to near-surface effects and those results are reported in Figure S4a–f, Supporting Information. Chemical fingerprints of Si, O, and N were specifically investigated for the sample going through annealing and light-soaking cycles and for the sample considered as a reference that was left undisturbed and stored in dark ambient conditions directly after the deposition. The Si elemental peak around 99.4 eV reduced and a shoulder peak around 103.5 eV appeared corresponding to Si–O (Si 2p) during this experiment for both samples. At the same time, the finger print peak of O (1s) around 532.6 eV corresponding to Si–O chemistry appeared clearly. This was barely visible for the as-deposited samples. It can be concluded that the surface of the a-Si:H oxidized and saturated over time considering the reference sample (Figure S4a–d,b–e, Supporting Information). The sample that went through annealing and light soaking showed a higher oxidized state that can be related to high-intensity light-induced oxidation when compared to the reference sample.[29] In addition, the reference sample going through surface oxidation over time also corroborates the observation made in Figure 2a, with the measured spontaneous blue-shift over the aging period after first annealing step when the AR coating was left in ambient conditions (Figure S4d,e, Supporting Information). Therefore, it can be concluded that the Si–O related FTIR and XPS measurements corroborate the surface oxidation. Although annealing was performed in N$_2$ environment, no N chemical fingerprints were found for either of these samples (Figure S4c,f, Supporting Information) nor any change in oxidation post-annealing was observed. Multiple steps of annealing can potentially crystallize the a-Si:H film to some extent. Hence, Raman spectroscopy measurements were performed as this technique is popularly used with a-Si:H thin-film analysis to determine the crystalline volume fraction.[45] The measurements show no discernible change after cycles of annealing and light soaking (Figure S5, Supporting Information). Therefore, the amorphous character of the a-Si:H film was fully preserved during the cycles of annealing and prolonged high-intensity light soaking, which underlines that the optical programmability of the material can be preserved when using moderate annealing temperatures.

Loss of hydrogen in the a-Si:H film was reported to cause a reduction in the effective refractive index.[46,47] Also, surface oxidation can reduce the effective refractive index.[13,29,48] The initial slow blue-shift can be related to oxidation of the

ADVANCED
SCIENCE NEWS
www.advancedsciencenews.com

ADVANCED
OPTICAL
MATERIALS
www.advopticalmat.de

pristine surface of the resonant device that causes a decrease of the effective refractive index of a-Si:H. The annealing-induced initial blue-shift can be related to the reduced refractive index of the a-Si:H film. In addition, the saturation of the excess blue-shift after several annealing treatments may be related to the eventual saturation of the loss of hydrogen. Therefore, these initial irreversible steps can be tied to the loss of hydrogen and surface oxidation. Since these phenomena subside with repeating cycles, the reversibility between annealing and light soaking appears clearly in later cycles as would be desirable for using this material in a PIC.

2.2. A Reconfigurable Optical Switch with a-Si:H

An MRR device was chosen for exploiting the metastable refractive index property of a-Si:H and to demonstrate a reconfigurable photonic device. An MRR is a versatile photonic integrated device that has been suggested as a building block for optical filters, memory elements, and optical switches.[9,15,49–53] The schematic of the MRR and the scanning electron microscope (SEM) image of its constituent waveguide cross-section are shown in **Figure 3**a. The waveguides were designed to be 510 nm in width and 220 nm in height for the propagation of fundamental TE-like mode. The a-Si:H-based MRR devices were patterned using an electron beam lithography (EBL) system. The SEM image of the fabricated ring resonator device with a diameter of 50 μm is shown in Figure 3b. The devices were entirely made of a-Si:H and have only air cladding. Among the fabricated

devices, two devices with high Q (Q-factor = resonant wavelength/full width at half maximum (FWHM) ≈ 1×10^4) were chosen to study the effects of annealing and light soaking. The measured as-fabricated response from one of these MRRs is shown in Figure S6, Supporting Information. Besides the characteristic repetitive resonant dips, an additional dip from the fiber Bragg grating nanometer is seen at 1546.9 that serves as a reference for measurements. The MRR resonant wavelength is proportional to the effective refractive index of the waveguide and radius of the ring ($m \lambda_{res} = 2\pi r n_{eff}$). Therefore, any change in the effective refractive index as perceived above is supposed to shift the resonant wavelengths accordingly. The shift of one such resonance (marked in Figure S6, Supporting Information) during cycles of annealing and light soaking was investigated. The resonant wavelength from this figure is extracted and reported in Figure 3c.

The resonance wavelength of as-fabricated MRR at 1536.70 nm irreversibly blue-shifted by 1.50 nm including the second annealing step (first cycle annealing and light soaking and then annealing again) and the resonance reaches 1535.20 nm. Similar to the thin-film interferometry experiment, the initial irreversibility is observed during the first three steps. Subsequently, light soaking reversed, that is, red-shifted the resonance to 1535.45 nm. Proceeding with cycles of annealing and light soaking showed a similar reversible nature as shown with the thin-film interferometry experiment. Additionally, the excess drift after annealing and the repeatability of the reversibility improved from the third cycle of light soaking onward as also observed in the previous experiment. Therefore, these
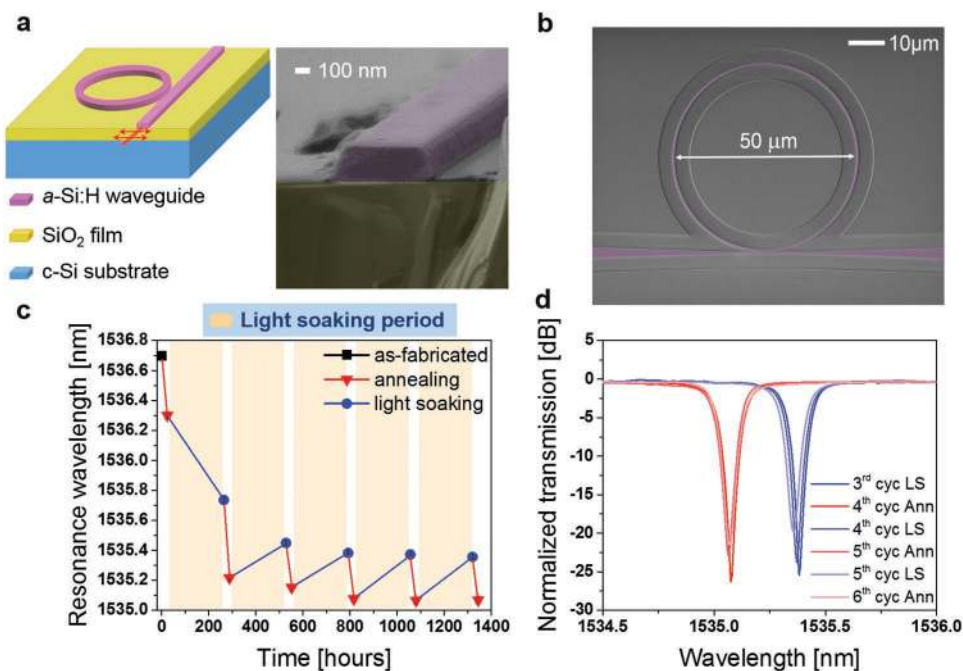
Figure 3. Effect of cycles of annealing and light soaking on the a-Si:H-based photonic micro-ring resonator (MRR). a) Simple schematic representation of the fabricated MRR is shown with the cross-section SEM image of the constituent waveguide. The waveguide structure is designed to be 510 nm wide and 220 nm thick a-Si:H on SiO₂ to facilitate fundamental TE-mode propagation. b) SEM image of the fabricated 50 μm diameter MRR (highlighted in pink) with two tapered waveguides to access the MRR. c) Investigation of the resonance wavelength shift after cycles of annealing and light soaking. d) The switching condition of the MRR after repeatable reversibility was achieved between the annealed and light-soaked states (1 cycle = one annealing and one light-soaking treatment, cyc, cycle; Ann, annealing; LS, light soaking).

switching states can be reconfigured for multiple cycles as shown here up to three cycles. This demonstration supports the SWE studies performed for solar cells, as it was demonstrated that after the initial onset of the irreversible regime, the reversible regime can be accessed over many subsequent reversible cycles.[38,54] Figure 3c shows that the resonance wavelength was reversibly shifting by 0.3 nm between the annealed and light-soaked states of the MRR for the resonance under investigation as well as for periodical resonances (see Figure S7a, Supporting Information). These switching states can be potentially reconfigured for multiple cycles as shown here up to four cycles. The optical switching states are well defined with an on/off extinction ratio greater than 20 dB and an unchanged FWHM as shown in Figure 3d. The Q-factor remained unchanged while switching between annealed and light-soaked states (see Figure S7b, Supporting Information). As the device performance remains unchanged between switching states, it is expected that there is a negligible change in the imaginary part of the refractive index (absorption). Hence, the reversible resonance shift observed here is due to the change in the real part of the refractive index as determined from the thin-film interferometric experiment. This is unlike the O-PCM-based switching devices, where high optical losses, related to the crystalline state of O-PCM, compromise the performance of the MRR switching states.[9,19,52] From the reversible resonant wavelength shift ($\Delta\lambda_{res}$), the effective refractive index change (Δn_{eff}) can be estimated by the following equations

$$\Delta n_{eff} = \frac{n_g \times \Delta\lambda_{res}}{\lambda_{res}} \quad \text{and} \quad n_g = \frac{\lambda_{res}^2}{FSR \times L} \tag{1}$$

where n_g denotes the group index of the waveguide, L represents the round trip path length, and FSR (free spectral range) corresponds to the period gap between resonant wavelengths.[55] We estimated that the effective refractive index reversibly changes by 0.8×10^{-3} that is comparable to what was estimated by the thin-film interferometric technique. However, the initial irreversibility shift observed for thin-film interferometry experiment was 4.75 nm, while it was 1.5 nm for the MRR. This difference may be related to the fact that the MRR went through multiple processing steps during fabrication compared to the thin-film AR coating. Other than this, there is a striking similarity between the thin-film interferometry experiment and the MRR-based optical switch. A similar observation is made for a second MRR on the same chip that was investigated as well (see Figure S7c, Supporting Information). On the short-term, the thin-film AR coatings appeared stable after light soaking and annealing. Therefore, the fabricated MRR was used to further investigate the long-term stability while the device was stored in the dark at room temperature. It was observed that with time, the device showed a continuous red-shift, that is, drift from the programmed state. This continuous unidirectional drift was observed after both the annealed and light-soaked states (details in Section 8, Supporting Information). However, the aging-related drift kinetics (2.62×10^{-4} nm h^{-1}) are much slower compared to the light-induced red-shift (1.24×10^{-3} nm h^{-1}). Also, light soaking showed a repeated saturating effect from the thin-film interferometric experiment, unlike the continuous slow drift. Therefore, it is likely that the drift is related to the specific waveguide structure or its constituent material stack and dimensions.

2.3. Freestanding Thin-Film Membrane for Strain Analysis

In order to understand the origin of the demonstrated reversible refractive index changes between annealing and light soaking as well as to further explore the stability, we performed an experiment with a-Si:H freestanding thin-film membrane. We studied the strain changes in the membrane during cycles of annealing and light soaking, as a change of strain in the film will yield a change in the membrane profile. For this experiment, 220 nm thick a-Si:H membranes of specific bridge-like freestanding features were fabricated as shown in **Figure 4**a (complete fabrication process is detailed in Section 10, Supporting Information). The bridges were 365 µm in length and 10–15 µm in width. As soon as the membranes were released, they expanded in the upward direction, which is clearly evident in the SEM image of one such structure (Figure 4b). The expansion of the freestanding membrane is indicative of compressive stress that is a typical characteristic of a-Si:H deposited by plasma-enhanced processes.[56] Consequently, the changes are pronounced in one plane making them easier to study. The measured spatial profile of one such bridge is shown in Figure 4c and as measured using a 3D optical profiler (Bruker NPFLEX). The extracted line profile across the freestanding bridge (white dashed line in Figure 4c) is shown in Figure 4d. The peak height of the as-fabricated freestanding membrane of 365 µm in length and 15 µm in width is 10.43 µm.

The freestanding membrane was subjected to cycles of annealing and light soaking. The annealing conditions are the same as in the thin-film interferometry experiment. The light-soaking treatment was limited to 168 h (7 days) since it was observed in the previous experiments to be sufficient time to reach saturation. Changes in the freestanding membrane profile magnified around the peak during three cycles of annealing and light soaking are presented in **Figure 5**a. It is clear that the peak height of the freestanding membrane changed between the annealed and light-soaked states and the differences between them are distinctly visible. The peak heights were extracted and reported in Figure 5b. The as-fabricated peak height changed from 11.65 to 10.50 µm after annealing. After the light soaking, the peak height recovered back to 11.73 µm. During the subsequent cycles of annealing and light soaking, the peak heights changed reversibly between 11.00 and 11.30 µm, which is not the same as the first cycle. Generally, it was observed that the light soaking increased the peak height that yielded an expansion of the membrane, while annealing decreased the peak height and resulted in a contraction of the membrane. This is in line with the previous observations that light-soaking treatment increases the intrinsic stress and annealing decreases the stress in the a-Si:H film.[26,27] The reversible peak height change is 300 ± 30 nm. Similar changes in the membrane profile and height were observed for another membrane structure (length 365 µm and width 10 µm) during cycles of annealing and light soaking as shown in Figure S11, Supporting Information.

By a simple first-order linear fitting of the line profiles, we extracted the excess length change (Δl) due to the expansion
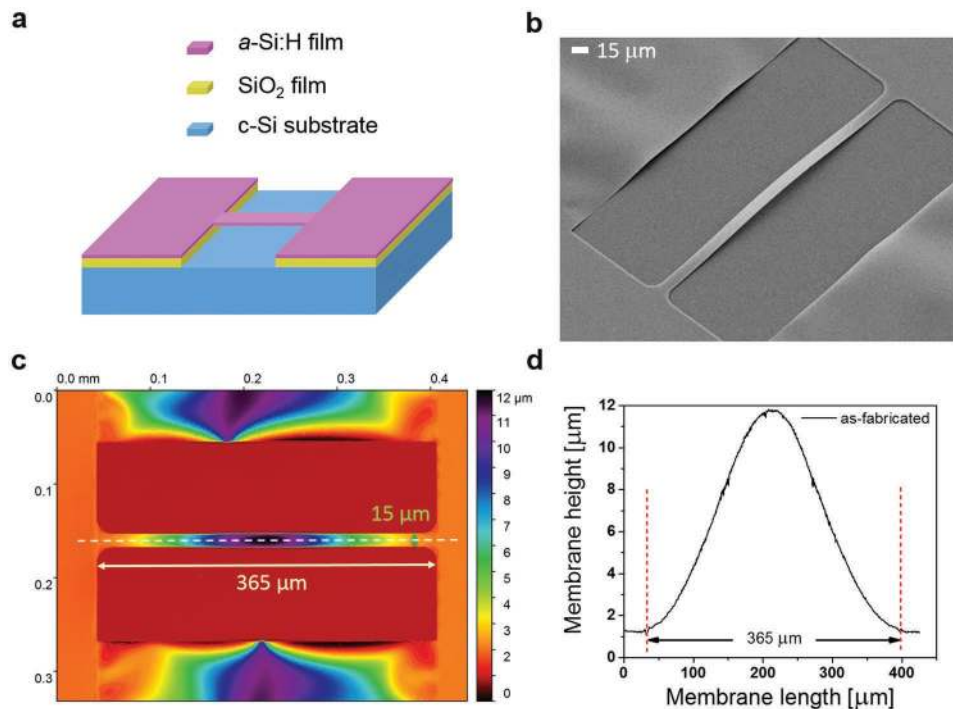
Figure 4. a-Si:H freestanding thin-film membrane to study the effects of cycles of annealing and light soaking treatments on strain correlated to the observed refractive index change. a) A simple schematic of the fabricated freestanding bridge structure by patterning and dry etching of a-Si:H (around 220 nm) and then wet etching of sacrificial SiO$_2$ (around 1 µm). b) SEM image of the freestanding bridge shown here buckles upward due to the high compressive stress in the a-Si:H film. c) Using an optical profiler, the spatial profile of the freestanding a-Si:H bridge was measured for a 365 µm in length and 15 µm in width bridge. d) The extracted line profile that goes across the bridge as shown by the dashed white line in panel (c). The free-standing membrane has a peak height of 10.43 µm from the film plane and 11.65 µm from the crystalline silicon substrate.
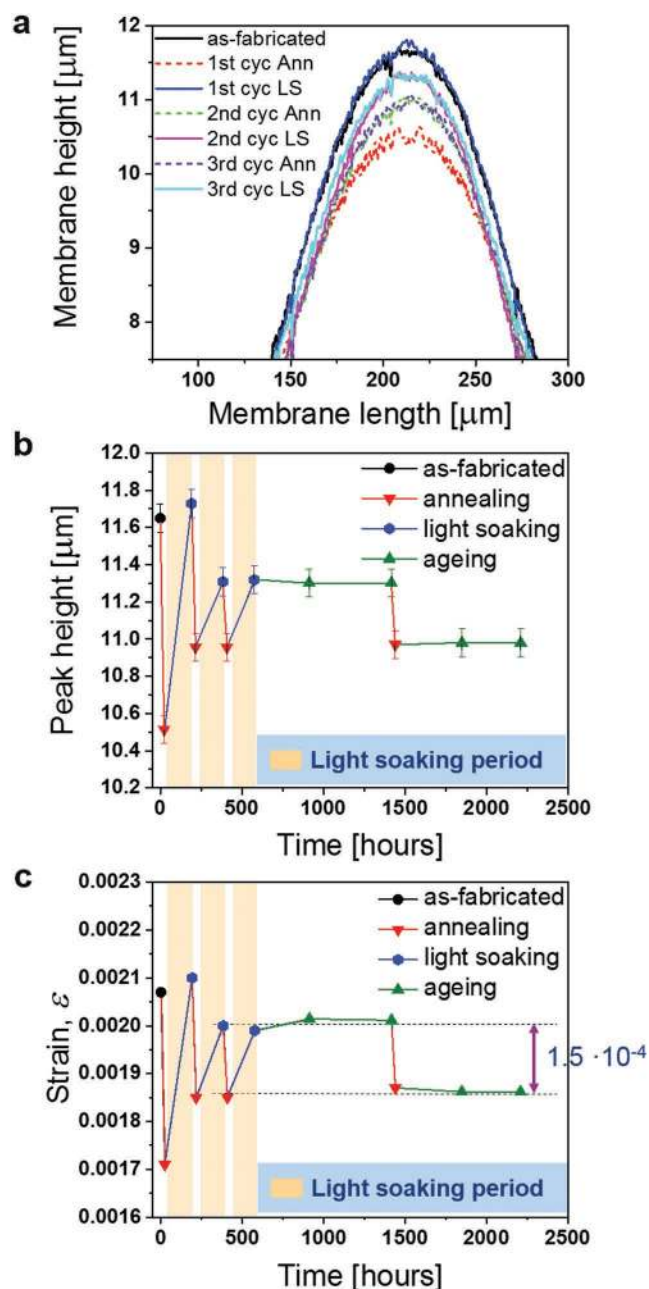
and contraction of the membrane. From a base length of the membrane (l), we derived the strain, $\varepsilon(= \Delta l/l)$ and monitor the changes therein during cycles of annealing and light soaking, as shown in Figure 5c. Similar to the thin-film interferom-etry experiment and MRR response, the initial irreversibility persists until the second annealing step (first cycle annealing and light soaking and then annealing again) when compared to the follow-up steps. However, this initial irreversibility was not one-directional as observed from the previous experiments. This is an unclear aspect, as it is difficult to fully understand the effects of surface oxidation and initial loss of hydrogen in addition to annealing and light soaking that affect the intrinsic strain in the freestanding membrane. In the reversible regime, it was approximated that the strain of the membrane increases by 1.5×10^{-4} compared to its annealed state. Interestingly, the light-induced increase of strain can be related to the increased effective refractive index as consistently observed in our experi-ments, since the increase of strain is reported to increase the refractive index.[57,58] It was reported that the strain increase by applied external force in the order of 10^{-4} results in 0.1 nm red-shift for c-Si-based MRR.[58] It is possible that the strain change under similar conditions can be different for mem-brane-like (freestanding) thin-films and substrate-bonded thin-films. Therefore, we cannot make a direct comparison between the refractive index change observed for the MRR device or AR coating and the membrane strain change. However, the demonstrated results present a reasonable similarity between strain change and refractive index change, that is, a device

performance shift under applied strain, as has been reported elsewhere.[58,59]

In addition, it is interesting to note that, both the annealed and light-soaked states were retained at least up to 1 month. The stability of the programmed state confirms the funda-mental nature of the metastable SWE. As proposed earlier, the observed unstable nature can indeed be related to the specific geometry and the layer stack of the device. Aging of the MRR showed only a red-shift, which can be associated with an increase of strain over time. The exposed SiO$_2$ around the waveguide may contribute toward the observed effect. Post-annealing stress instability issues with aging of SiO$_2$ have been reported.[60,61] On the other hand, similar red-shifting instability in SOI-based MRR response has been reported after imparting electron-beam-induced compaction. It has been also suggested that 200–400 nm light can cause similar compaction of the SiO$_2$ layer.[62] Therefore, prolonged exposure to high-intensity source that emits light close to 400 nm may contribute to the observed instability. However, this issue requires further investiga-tion in order to identify the specific reason and come up with ways to mitigate the drift. The fact that the membranes were stable suggests that their application in reconfigurable photonic devices can come within reach if the devices are made with air-suspended waveguides.[63]

This demonstration of metastable a-Si:H based reconfig-urable photonic devices has the potential to address a multi-tude of photonic applications. This programming technique can be suitable for realizing trimming and fine-tuning of

**ADVANCED
SCIENCE NEWS**
www.advancedsciencenews.com

**ADVANCED
OPTICAL
MATERIALS**
www.advopticalmat.de

Figure 5. a-Si:H freestanding thin-film membrane peak height changing during cycles of annealing and light soaking treatments. a) The membrane line profile after annealing and light soaking cycles focused around the peak (1 cycle = 1 annealing and 1 light-soaking treatments, cyc, cycle; Ann, annealing; LS, light soaking). b) Reversible changes in the extracted peak heights from panel (a) were observed between annealing and light soaking. c) Strain change in the membrane corresponding to cycles of annealing and light soaking states. Reversible strain and stable strain changes in the freestanding membrane were observed. The "aging" data points (green triangles) correspond to measurements on the membrane after light soaking and annealing steps to assess the stability of the annealed and light-soaked states as the sample was stored in the dark and the ambient conditions.

photonic devices for tackling fabrication-related errors. Also, a linear combination of reconfigurable photonic switches can be employed and then locally programmed to obtain a specific functionality.[1,2,64,65] One can assume, a generic a-Si:H-based PIC template packaged after post-fabrication process with local heating elements and LED arrays assembled on PIC. The post-fabrication process includes a few cycles of light soaking and annealing to reach the reversible light-soaked state. Thereafter, the local heating elements can individually tune devices to obtain a desired PIC functionality. The programmed functionality will not require any additional power consumption or control circuitry as it is supported by the metastable nature of a-Si:H.[2,4] Additionally, it will be possible to reuse the same template by light soaking it, by which the programmed state will be erased to allow additional reprogramming of the PIC's functionality. This concept still needs to be verified in terms of the attainable reversible magnitude of programmability, the required time for programming, and long-term stability. It is clear that a-Si:H material properties, that is, hydrogen content, bandgap, microstructure, intrinsic stress, etc. can be widely tuned based on deposition conditions.[29,40,56,66–68] Therefore, it may be possible to improve the magnitude of reversibility by tuning the hydrogen content and the intrinsic stress as these two properties have been suggested to be correlated with metastable volumetric expansion.[26,69] In addition, wavelength, the intensity of light and mode of illumination (continuous or pulsed), has been also suggested to affect the light-induced saturation time for metastable volumetric expansion.[26] Also, spike annealing conditions can be realized and optimized with on-chip heating elements that can potentially reduce the annealing time required for programming.[54] These are some of the possible avenues to be explored for improving the magnitude of the metastable refractive index reversibility and shortening the programming time to realize practical a-Si:H-based programmable multipurpose passive PICs. Additionally, the non-volatile and reversible shape-changing properties of a-Si–H freestanding membranes can potentially open a new route toward reconfigurable metamaterials and novel optomechanical devices.[70,71]

3. Conclusion

We devised a sophisticated interferometric technique to study the changes in the optical properties of a-Si:H due to cycles of annealing and light soaking. It is convincingly demonstrated that a-Si:H exhibits a light-induced metastable refractive index change by 0.3% ($\Delta n \approx 0.001$) that is reversible upon annealing. We further demonstrated a metastable optical switch in the form of a MRR based on a-Si:H that is fully reconfigurable between the annealed and light-soaked states over multiple programming cycles. The switching states are well separated by 0.3 nm and the extinction ratio between the switched states was maintained at >20 dB. To better understand the origin of the optical metastability and device instability, we devised an experiment with an a-Si:H-based freestanding membrane. It is established that a light-induced strain modulation in the a-Si:H freestanding thin-film membrane during annealing and light soaking, also known as metastable volumetric expansion, is the main contributor to the observed phenomena. Also, the membrane exhibited stability of the programmed states, suggesting a potential route to making metastable photonic devices. Because

**ADVANCED
SCIENCE NEWS**
www.advancedsciencenews.com

**ADVANCED
OPTICAL
MATERIALS**
www.advopticalmat.de

the observed effect is metastable in nature, there is no need for continuous stimulation and no distinguishable changes in the optical losses were observed, as mainly the real part of the refractive index is affected. Furthermore, possible routes toward improving reconfigurable devices with metastable a-Si:H are also discussed. Fine-tuning of the reversibility, magnitude, and stability of this metastable refractive index is foreseen to lead to a-Si:H-based reconfigurable photonics that support multi-purpose reconfigurable photonic chips, reconfigurable meta-materials, and optomechanical devices. This demonstration is the first step toward a new generation of metastable a-Si:H based, non-volatile, and reconfigurable photonic devices and integrated circuits.

4. Experimental Section

Thin-Film Interferometer Sample Preparation and Measurement: Crystalline silicon (<100> crystal orientation, undoped, SSP, and 280 µm thickness) was used as a substrate. The substrate was cleaned in 1% HF for 1 min. Subsequently, 119.5 ± 0.5 nm silicon oxide was deposited using a plasma-enhanced chemical vapor deposition (PECVD) reactor Plasmalab System 100 from Oxford Instruments. The SiO_2 layer was deposited at 300 °C deposition temperature, 1000 mTorr pressure, and 20 W plasma power to dissociate 8.5 sccm silane (SiH_4), 161.5 sccm nitrogen (N_2), and 710 sccm nitrous oxide (N_2O) flow. The typical deposition rate was 1.18 nm s^{-1}. The deposited SiO_2 was annealed at 900 °C in vacuum for an hour with a rapid thermal annealing system by Jipelec JetFirst. After this post-deposition annealing, 265 ± 0.6 nm a-Si:H was deposited on SiO_2 with an inductively coupled PECVD Plasmalab 100 system. Silane (SiH_4) precursor gas was diluted with argon (Ar) gas for deposition. The flow rate of SiH_4 and Ar were 12 and 48 sccm, respectively. The plasma power was 600 W and the pressure during the deposition was maintained at 10 mTorr. The deposition temperature was 80 °C. For these deposition conditions, the typical deposition rate was 0.14 nm s^{-1}. A Keysight 81980A (1465–1575 nm) tunable laser was used and scanned with 0.1 nm steps for the reflectance measurement. The wavelength corresponding power was measured using a Keysight 81532A power meter. Thorlabs F260FC-1550 3 mm beam collimators were used to launch and collect the light. A Newport 10LP-NIR polarization filter with 30 dB polarization extinction ratio was used. A polarization filter and collimators were mounted on a Newport M-RS65 rotation stage for optimum polarization control.

Material Characterization: Film thickness, deposition rate, and optical properties were determined by SE using a J.A. Woollam Co. M2000D rotating compensator. The measurement spectrum was between 196 and 1000 nm at different angles, that is, 65°, 70°, and 75°. The SiO_2 layer was modeled with a Cauchy dispersion relation. The a-Si:H layer was modeled with a Tauc–Lorentz oscillator.[72] The analysis was done using the proprietary software CompleteEA SE. Consistency in the Si- and O-bonded hydrogen content in the film after every annealing step in the experiment was done by a Bruker Tensor 27 FTIR spectrometer. The measurements were done in transmission mode between 340 and 7000 cm^{-1}. The hydrogen content of the as-deposited a-Si:H film was determined from an FTIR measurement to be 20.5% and the microstructure parameter, $R*$, was 0.21.[29] The crystallinity in the film was investigated using Raman spectroscopy using a Renishaw inVia Raman microscope. The measured signals were acquired in backscattering geometry and data acquired between 100 and 900 cm^{-1}. The Raman signal was excited using a 514 nm laser. Measurement parameters were chosen to be 1% of the laser power with 10 scans of 10 s for each measurement after carefully checking that the crystallinity of the film remained unaffected by the laser.

Light Soaking and Annealing: The light-soaking treatments on the samples were done using a home-built setup with a concentrated LED 4000 K cool white source. The power intensity was determined to be 470 mW cm^{-2} using a pyranometer (LSI LASTEM). The measured spectrum of the lamp showed that photons are emitted in the 410–800 nm range (see Figure S2, Supporting Information). The sample holder was water cooled at 20 °C during the light-soaking treatment. Annealing was performed in a vacuum oven at 180 °C for 4 h in an N_2 environment. The ramping condition was 5 °C min^{-1} and the system convectively cooled down to room temperature before opening the oven.

Freestanding Thin-Film Membrane Preparation and Measurement: Complete fabrication process steps are detailed in Section 10, Supporting Information. The fabricated freestanding membrane structures (bridges) were studied with a 3D optical profiler (Bruker NPFLEX). The measurements recorded the state of the 3D membrane profile after fabrication and cycles of annealing and light soaking.

Fabrication of Photonic Integrated Device: Crystalline silicon wafers (<100> orientation, 525 µm thick, 10 Ωcm, p-type, SSP) with 2 µm wet thermal oxide (Siegert Wafer) were used for the photonic device fabrication. Two hundred twenty nanometers a-Si:H was deposited with the same deposition conditions as stated above. An EBL system (Raith EBPG5150 100 kV) was used to pattern the devices on ZEP 520A photoresist that was developed in *n*-amyl acetate for 80 s and rinsed in MIBK-IPA (1:2) solution for 60 s. A reactive ion-etching system was used to dry etch a-Si:H with an Oxford Instruments Plasmalab 100 PECVD system. The etching was conducted using 100 W plasma power, at a pressure of 15 mTorr, and using 60 sccm CHF_3. ZEP photoresist was used as a mask for the etching process. After etching, the photoresist was removed completely with an O_2 plasma treatment (50 W plasma power, 15 mTorr, and 20 sccm O_2 flow) for 5 min. The device was tested through fiber grating couplers using a vertical coupling setup and details are presented in Section 9, Supporting Information. Light soaking was done for 10 days while the other conditions were the same as described above. Annealing conditions were the same as described above.

Supporting Information

Supporting Information is available from the Wiley Online Library or from the author.

Conflict of Interest

The authors declare no conflict of interest.

[1] O. Graydon, *Nat. Photonics* **2016**, *10*, 1.

[2] J. Capmany, I. Gasulla, D. Pérez, *Nat. Photonics* **2016**, *10*, 6.

[3] W. Liu, M. Li, R. S. Guzzon, E. J. Norberg, J. S. Parker, M. Lu, L. A. Coldren, J. Yao, *Nat. Photonics* **2016**, *10*, 190.

[4] D. Pérez, I. Gasulla, L. Crudgington, D. J. Thomson, A. Z. Khokhar, K. Li, W. Cao, G. Z. Mashanovich, J. Capmany, *Nat. Commun.* **2017**, *8*, 1.

[5] N. C. Harris, G. R. Steinbrecher, M. Prabhu, Y. Lahini, J. Mower, D. Bunandar, C. Chen, F. N. C. Wong, T. Baehr-Jones, M. Hochberg, S. Lloyd, D. Englund, *Nat. Photonics* **2017**, *11*, 447.

[6] J. Carolan, C. Harrold, C. Sparrow, E. Martín-López, N. J. Russell, J. W. Silverstone, P. J. Shadbolt, N. Matsuda, M. Oguma, M. Itoh, G. D. Marshall, M. G. Thompson, J. C. F. Matthews, T. Hashimoto, J. L. O'Brien, A. Laing, *Science* **2015**, *349*, 711.

[7] Y. Shen, N. C. Harris, S. Skirlo, M. Prabhu, T. Baehr-Jones, M. Hochberg, X. Sun, S. Zhao, H. Larochelle, D. Englund, M. Soljacic, *Nat. Photonics* **2017**, *11*, 441.

[8] C. García-Meca, S. Lechago, A. Brimont, A. Griol, S. Mas, L. Sánchez, L. Bellieres, N. S. Losilla, J. Martí, *Light: Sci. Appl.* **2017**, *6*, e17053.

[9] C. Rios, P. Hosseini, C. D. Wright, H. Bhaskaran, W. H. P. Pernice, *Adv. Mater.* **2014**, *26*, 1372.

[10] P. Hosseini, C. D. Wright, H. Bhaskaran, *Nature* **2014**, *511*, 206.

[11] M. M. Milosevic, X. Chen, W. Cao, A. F. J. Runge, Y. Franz, C. G. Littlejohns, S. Mailis, A. C. Peacock, D. J. Thomson, G. T. Reed, *IEEE J. Sel. Top. Quantum Electron.* **2018**, *24*, 1.

[12] A. Canciamilla, S. Grillanda, F. Morichetti, C. Ferrari, J. Hu, J. D. Musgraves, K. Richardson, A. Agarwal, L. C. Kimerling, A. Melloni, *Opt. Lett.* **2011**, *36*, 4002.

[13] Y. Shen, I. B. Divliansky, D. N. Basov, S. Mookherjea, *Opt. Lett.* **2011**, *36*, 2668.

[14] M. Wuttig, H. Bhaskaran, T. Taubner, *Nat. Photonics* **2017**, *11*, 465.

[15] C. Ríos, H. Bhaskaran, C. D. Wright, W. H. P. Pernice, D. Wang, T. Scherer, M. Stegmaier, P. Hosseini, *Nat. Photonics* **2015**, *9*, 725.

[16] P. Xu, J. Zheng, J. K. Doylend, A. Majumdar, *ACS Photonics* **2019**, *6*, 553.

[17] K. J. Miller, R. F. Haglund, S. M. Weiss, *Opt. Mater. Express* **2018**, *8*, 2415.

[18] W. Dong, H. Liu, J. K. Behera, L. Lu, R. J. H. Ng, K. V. Sreekanth, X. Zhou, J. K. W. Yang, R. E. Simpson, *Adv. Funct. Mater.* **2019**, *29*, 1806181.

[19] J. Zheng, A. Khanolkar, P. Xu, S. Colburn, S. Deshmukh, J. Myers, J. Frantz, E. Pop, J. Hendrickson, J. Doylend, N. Boechler, A. Majumdar, *Opt. Mater. Express* **2018**, *8*, 1551.

[20] Y. Zhang, J. B. Chou, J. Li, H. Li, Q. Du, A. Yadav, S. Zhou, M. Y. Shalaginov, Z. Fang, H. Zhong, C. Roberts, P. Robinson, B. Bohlin, C. Ríos, H. Lin, M. Kang, T. Gu, J. Warner, V. Liberman, K. Richardson, J. Hu, *Nat. Commun.* **2019**, *10*, 1.

[21] D. L. Staebler, C. R. Wronski, *Appl. Phys. Lett.* **1977**, *31*, 292.

[22] M. Stutzmann, W. B. Jackson, C. C. Tsai, *Phys. Rev. B* **1985**, *32*, 23.

[23] A. Yelon, A. Rochefort, S. Sheng, E. Sacher, *Sol. Energy Mater. Sol. Cells* **2003**, *78*, 391.

[24] D. Han, J. Baugh, G. Yue, Q. Wang, *Phys. Rev. B* **2000**, *62*, 7169.

[25] D. R. Queen, X. Liu, J. Karel, Q. Wang, R. S. Crandall, T. H. Metcalf, F. Hellman, *Europhys. Lett.* **2015**, *112*, 26001.

[26] P. Tzanetakis, *Sol. Energy Mater. Sol. Cells* **2003**, *78*, 369.

[27] T. Gotoh, S. Nonomura, M. Nishio, S. Nitta, M. Kondo, A. Matsuda, *Appl. Phys. Lett.* **1998**, *72*, 2978.

[28] N. Hata, P. Stradins, C. Fortmann, H. Fujiwara, M. Kondo, A. Matsuda, *J. Non-Cryst. Solids* **2000**, *266–269*, 491.

[29] M. A. Mohammed, J. Melskens, R. Stabile, W. M. M. Kessels, O. Raz, *Phys. Status Solidi A* **2018**, *215*, 1700754.

[30] M. Stuckelberger, R. Biron, N. Wyrsch, F. J. Haug, C. Ballif, *Renewable Sustainable Energy Rev.* **2017**, *76*, 1497.

[31] J. Melskens, A. H. M. Smets, M. Schouten, S. W. H. Eijt, H. Schut, M. Zeman, *IEEE J. Photovoltaics* **2013**, *3*, 65.

[32] J. Melskens, S. W. H. Eijt, M. Schouten, A. S. Vullers, A. Mannheim, H. Schut, B. Macco, M. Zeman, A. H. M. Smets, *IEEE J. Photovoltaics* **2017**, *7*, 421.

[33] J. Melskens, A. Schnegg, A. Baldansuren, K. Lips, M. P. Plokker, S. W. H. Eijt, H. Schut, M. Fischer, M. Zeman, H. M. Smets, *Phys. Rev. B* **2015**, *91*, 245207.

[34] S. J. Orfanidis, Electromagnetic Waves and Antennas, Rutgers University, New Jersey, http://eceweb1.rutgers.edu/~orfanidi/ewa/ (accessed: October 2018).

[35] J. A. Dobrowolski, in *Handbook of Optics: Fundamentals, Techniques, and Design* (Eds: M. Bass, E. W. V. Stryland, D. R. Williams, W. L. Wolfe), McGraw-Hill, New York **1995**.

[36] Z. Ni, S. Mou, T. Zhou, Z. Cheng, *Appl. Opt.* **2018**, *57*, 3385.

[37] S. Yoo, T. Gwon, T. Eom, S. Kim, C. S. Hwang, *ACS Photonics* **2016**, *3*, 1265.

[38] E. M. El Mhamdi, J. Holovsky, B. Demaurex, C. Ballif, S. De Wolf, *Appl. Phys. Lett.* **2014**, *104*, 252108.

[39] A. H. M. Smets, M. C. M. van de Sanden, *Phys. Rev. B* **2007**, *76*, 073202.

[40] A. H. M. Smets, W. M. M. Kessels, M. C. M. van de Sanden, *Appl. Phys. Lett.* **2003**, *82*, 1547.

[41] J. Melskens, A. H. M. Smets, S. W. H. Eijt, H. Schut, E. Brück, M. Zeman, *J. Non-Cryst. Solids* **2012**, *358*, 2015.

[42] E. San Andrés, A. Del Prado, F. L. Martínez, I. Mártil, D. Bravo, F. J. López, *J. Appl. Phys.* **2000**, *87*, 1187.

[43] K. Ka-Hyun, E. V. Johnson, P. R. I. Cabarrocas, *Jpn. J. Appl. Phys.* **2016**, *55*, 072302.

[44] F. Kail, S. Fellah, A. Abramov, A. Hadjadj, P. Roca i Cabarrocas, *J. Non-Cryst. Solids* **2006**, *352*, 1083.

[45] C. Smit, R. A. C. M. M. van Swaaij, H. Donker, A. M. H. N. Petit, W. M. M. Kessels, M. C. M. van de Sanden, *J. Appl. Phys.* **2003**, *94*, 3582.

[46] S. K. Selvaraja, W. Bogaerts, D. VanThourhout, M. Schaekers, *Appl. Phys. Lett.* **2010**, *97*, 071120.

[47] T. Lipka, M. Kiepsch, H. K. Trieu, J. Müller, *Opt. Express* **2014**, *22*, 12122.

[48] B. Drevillon, F. Vaillant, *Thin Solid Films* **1985**, *124*, 217.

[49] R. A. Cohen, O. Amrani, S. Ruschin, *Nat. Photonics* **2018**, *12*, 706.

[50] J. Wang, H. Shen, L. Fan, R. Wu, B. Niu, L. T. Varghese, Y. Xuan, D. E. Leaird, X. Wang, F. Gan, A. M. Weiner, M. Qi, *Nat. Commun.* **2015**, *6*, 5957.

[51] S. Le Beux, Z. Li, C. Monat, X. Letartre, I. O'Connor, in *2013 IFIP/ IEEE 21st Int. Conf. on Very Large Scale Integration (VLSI-SoC)*, (Eds: M. Margala, R. Reis, A. Orailoglu, L. Carro, L. M. Silveira, H. F. Ugurdag), IEEE Xplore, Istanbul, Turkey **2013**, pp. 180–185.

[52] M. Rudé, J. Pello, R. E. Simpson, J. Osmond, G. Roelkens, J. J. G. M. van der Tol, V. Pruneri, *Appl. Phys. Lett.* **2013**, *103*, 141119.

[53] J.-F. Song, X.-S. Luo, A. E.-J. Lim, C. Li, Q. Fang, T.-Y. Liow, L.-X. Jia, X.-G. Tu, Y. Huang, H.-F. Zhou, G.-Q. Lo, *Sci. Rep.* **2016**, *6*, 1.

[54] M. J. M. Pathak, J. M. Pearce, S. J. Harrison, *Sol. Energy Mater. Sol. Cells* **2012**, *100*, 199.

[55] Q. Du, Y. Huang, O. Ogbuu, W. Zhang, J. Li, V. Singh, A. M. Agarwal, J. Hu, *Opt. Lett.* **2017**, *42*, 587.

[56] J. P. Harbison, A. J. Williams, D. V. Lang, *J. Appl. Phys.* **1984**, *55*, 946.

[57] J. Cai, Y. Ishikawa, K. Wada, *Opt. Express* **2013**, *21*, 7162.

[58] Y. Amemiya, Y. Tanushi, T. Tokunaga, S. Yokoyama, *Jpn. J. Appl. Phys.* **2008**, *47*, 2910.

[59] D. Taillaert, W. van Paepegem, J. Vlekken, R. Baets, *Third Eur. Work. Opt. Fibre Sensors*, (Eds: A. Cutolo, B. Culshaw, J. M. Lopez-Higuera), SPIE Digital Library **2007**, https://doi.org/10.1117/12.738412.

**ADVANCED
SCIENCE NEWS**

www.advancedsciencenews.com

**ADVANCED
OPTICAL
MATERIALS**

www.advopticalmat.de

[60] M. S. Haque, H. A. Naseem, W. D. Brown, *Thin Solid Films* **1997**, *308–309*, 68.

[61] C. Scalliet, L. Berthier, *Phys. Rev. Lett.* **2019**, *122*, 255502.

[62] J. Schrauwen, D. van Thourhout, R. Baets, *Opt. Express* **2008**, *16*, 3738.

[63] J. Soler Penades, A. Ortega-Moñux, M. Nedeljkovic, J. G. Wangüemert-Pérez, R. Halir, A. Z. Khokhar, C. Alonso-Ramos, Z. Qu, I. Molina-Fernández, P. Cheben, G. Z. Mashanovich, *Opt. Express* **2016**, *24*, 22908.

[64] A. Ribeiro, A. Ruocco, L. Vanacker, W. Bogaerts, *Optica* **2016**, *3*, 1348.

[65] L. Zhuang, C. G. H. Roeloffzen, M. Hoekman, K.-J. Boller, A. J. Lowery, *Optica* **2015**, *2*, 854.

[66] A. H. M. Smets, M. A. Wank, B. Vet, M. Fischer, R. A. C. M. M. van Swaaij, M. Zeman, D. C. Bobela, C. R. Wronski, R. M. C. M. van de Sanden, *IEEE J. Photovoltaics* **2012**, *2*, 94.

[67] K. Fukutani, M. Kanbe, W. Futako, B. Kaplan, T. Kamiya, C. M. Fortmann, I. Shimizu, *J. Non-Cryst. Solids* **1998**, *227–230*, 63.

[68] Q. Cheng, S. Xu, S. Huang, K. Ostrikov, *Cryst. Growth Des.* **2009**, *9*, 2863.

[69] S. Nonomura, N. Yoshida, T. Gotoh, T. Sakamoto, M. Kondo, A. Matsuda, S. Nitta, *J. Non-Cryst. Solids* **2000**, *266–269*, 474.

[70] N. I. Zheludev, Y. S. Kivshar, *Nat. Mater.* **2012**, *11*, 917.

[71] N. I. Zheludev, E. Plum, *Nat. Nanotechnol.* **2016**, *11*, 16.

[72] B. Macco, J. Melskens, N. J. Podraza, K. Arts, C. Pugh, O. Thomas, W. M. M. Kessels, *J. Appl. Phys.* **2017**, *122*, 035302.

1901680 (11 of 11)